Biochimica et Biophysica Acta 1830 (2013) 4229–4234

Contents lists available at SciVerse ScienceDirect

Biochimica et Biophysica Acta

journal homepage: www.elsevier.com/locate/bbagen

Configurational assignments of conformationally restricted bis-monoterpene hydroquinones: Utility in exploration of endangered plants

Joonseok Oh [a,1], John J. Bowling [a,1], Yike Zou [a], Amar G. Chittiboyina [b], Robert J. Doerksen [c], Daneel Ferreira [a], Theodor D. Leininger [d], Mark T. Hamann [a,*]

[a] Department of Pharmacognosy and Research Institute of Pharmaceutical Sciences, School of Pharmacy, The University of Mississippi, University, MS 38677, USA
[b] National Center for Natural Products Research, The University of Mississippi, Thad Cochran Research Center, University, MS 38677, USA
[c] Department of Medicinal Chemistry and Research Institute of Pharmaceutical Sciences, School of Pharmacy, The University of Mississippi, University, MS 38677, USA
[d] Center for Bottomland Hardwoods Research, USDA Forest Service, 432 Stoneville Road, Stoneville, MS 38776, USA

ARTICLE INFO

Article history:
Received 15 November 2012
Received in revised form 15 April 2013
Accepted 18 April 2013
Available online 26 April 2013

Keywords:
Configuration determination
Ab initio calculation
Conformation analysis
Natural product
NMR/CD spectroscopy
Endangered species

ABSTRACT

Background: Endangered plant species are an important resource for new chemistry. *Lindera melissifolia* is native to the Southeastern U.S. and scarcely populates the edges of lakes and ponds. Quantum mechanics (QM) used in combination with NMR/ECD is a powerful tool for the assignment of absolute configuration in lieu of X-ray crystallography.
Methods: The EtOAc extract of *L. melissifolia* was subject to chromatographic analysis by VLC and HPLC. Spin–spin coupling constant (SSCC) were calculated using DFT at the MPW1PW91/6-31G(d,p) level for all staggered rotamers. ECD calculations employed Amber* force fields followed by PM6 semi-empirical optimizations. Hetero- and homo-nuclear coupling constants were extracted from 1D ^{1}H, E.COSY and HETLOC experiments.
Results: Two meroterpenoids, melissifolianes A (1) and B (2) were purified and their 2-D structures elucidated using NMR and HRESIMS. The relative configuration of 1 was established using the combination of NOE-based distance restraints and the comparisons of experimental and calculated SSCCs. The comparison of calculated and experimental ECD assigned the absolute configuration of 1. The relative configuration of a racemic mixture, melissifoliane B (2) was established utilizing *J*-based analysis combined with QM and NMR techniques.**Conclusion** Our study of the *Lindera melissifolia* metabolome exemplifies how new chemistry remains undiscovered among the numerous endangered plant species and demonstrates how analysis by ECD and NMR combined with various QM calculations is a sensible approach to support the stereochemical assignment of molecules with conformationally restricted conformations.
General significance: QM–NMR/ECD combined approaches are of utility for unambiguous assignment of 3-D structures, especially with limited plant material and when a molecule is conformationally restricted. Conservation of an endangered plant species can be supported through identification of its new chemistry and utilization of that chemistry for commercial purposes.

1. Introduction

Endangered plant species are an underutilized resource for new chemistry. These discoveries ironically hold the potential for development into a commercial application that would justify the conservation of the plant. This is evidenced by a recent phylogenic analysis which shows drug producing plant families are concentrated around families which contain endangered species [1]. However, the challenge associated with such extraordinarily limited resources can prohibit the full elucidation of new structures through X-ray crystallography or NMR spectroscopy alone. The discovery of new bis-monoterpene hydroquinones from a U.S. endangered plant provides a unique opportunity in this regard. Owing to the conformationally restricted assemblies, the hydroquinones help demonstrate how combined quantum mechanical calculations with NMR and ECD studies can unambiguously assign three dimensional structures in cases where such detail might otherwise be lost due to limited resources.

Worldwide, at least 13% of the known flora is endangered or threatened [2] and the USDA verifies that 780 plant species in the U.S. and its territories are endangered or threatened [3]. Although several reports reveal the potential natural products from U.S. endangered species may provide [4], these reports are infrequent relative to

* Corresponding author. Tel.: +1 662 915 5730; fax: +1 662 915 6975.
E-mail address: mthamann@olemiss.edu (M.T. Hamann).
[1] These authors contributed equally to this manuscript.

0304-4165/$ – see front matter © 2013 Published by Elsevier B.V.
http://dx.doi.org/10.1016/j.bbagen.2013.04.029

the number of endangered U.S. species. Representative species of most of the U.S. endangered plant genera are distributed throughout the world. In some cases, the species have been investigated in regard to their unusual chemistry and traditional uses [4–7].

The endangered status of *Lindera melissifolia* (Walt.) Blume (Lauraceae), found in the Southeastern U.S., prompted our study of the plant as an example of how endangered U.S. plants can yield novel chemistry that could potentially be lost due to extinction. Commonly called pondberry, *L. melissifolia* is an aromatic and rhizomatous shrub that inhabits the edges of lakes and ponds. The essential oil from this plant possesses significant insect repellency [8]. The ethyl acetate extraction of pondberry drupes led to the discovery of two new bis-monoterpene hydroquinones named melissifolianes A (1) and B (2) (Fig. 1). The structures of the melissifolianes combine a common 2-(hydroquinone) acetic acid ester moiety flanked uniquely by two monoterpene units in contrast to a single monoterpene moiety as reported in *Magnolia denudata* [9]. The limited amounts of the melissifolianes negated assignment of their three dimensional structure by chemical methods or screening appropriate conditions for crystallization. However the conformationally restricted state associated with the monoterpene-linked acetic ester moiety provided the opportunity to employ computational methods to verify configuration. Herein, we report the use of NMR and ECD analysis coupled with quantum mechanical (QM) calculations for the establishment of configuration and conformation of natural products like the melissifolianes which contain conformationally restricted moieties.

2. Materials and methods

2.1. General procedures

NMR spectra were obtained using a Bruker Avance 400 MHz spectrometer referenced by residual dichloromethane and chloroform signals. Homo- and hetero-nuclear coupling constants were measured using ^{1}H-specturm, E.COSY (Exclusive COSY) and HETLOC (HETeronuclear LOng-range Coupling). Optical rotations were measured on a Rudolph Autopol V polarimeter. UV–vis spectra were recorded on an Agilent 1100 series diode array and multiple wavelength detectors (DAD). The LC–MS analyses were performed using an Agilent 1100 HPLC system with a Phenomenex Luna 5 μm C8(2) column (4.6 × 150 mm), an MeOH/H_2O (0.1% HCOOH) gradient solvent system and a Bruker Daltonics microTOF mass spectrometer or an Astec Chirobiotic R column (4.6 × 100 mm), 55% MeOH/H_2O isocratic condition (20 mM NH_4Ac, 35 °C) for the chiral separation. HRESIMS spectra were measured using the LC–MS system with electrospray ionization. Column chromatography was conducted using silica gel 60 (40–63 μm particle size) and RP-18 (40–63 μm particle size). Precoated TLC silica gel 60 F254 plates (Merck) were used for TLC. HPLC was performed on a Waters System equipped with a Waters 2487 dual absorbance detector. Experimental CD data was acquired at 5 °C using an Olis CD Spectrophotometer. The concentration of the sample was 500 μg/ml in MeCN and the path length was 5 mm.

2.2. Extraction and purification

Drupes (5 kg) of *L. melissifolia* were harvested in the Fall of 2009 at the Flooding Research Facility in Sharkey County, MS (Fig. S1-1). The dried ripe drupes of *L. melissifolia* were coarsely ground and extracted with EtOAc, and the extract was dried under reduced pressure to give 100 g of crude extract. The extract was fractionated on silica gel eluted sequentially by hexanes–EtOAc (100:0, 80:20, 50:50 and 0:100) and then EtOAc–MeOH (80:20, 50:50 and 0:100) to afford 10 fractions, respectively. Fractions 6–9 exhibited significant anti-infective activities and the active fractions were further chromatographed by normal phase [Phenomenex Luna Si, 10 × 250 mm, 5 μm, flow rate 5 mL/min] with a gradient elution of hexanes–EtOAc (1:0 to 8:2 over 120 min) and, finally, by reverse phase [Waters C_{18} 20 × 250 mm, 10 μm, flow rate 10 mL/min, Phenomenex C_{18} 5 × 250 mm, 5 μm, flow rate 1 mL/min] using a gradient elution of H_2O–MeOH (1:1 to 100% methanol over 110 min) to obtain the pure compounds.

2.2.1. Melissifoliane A (1)

Melissifoliane A (1, RT ≈ 46 min), (*R*)-methyl-2-{3-[(*E*)-3,7-dimethylocta-2,6-dien-1-yl]-2,5-dihydroxyphenyl}-2-[(1*S*,2*S*,5*S*)-2-hydroxy-5-isopropyl-2-methylcyclohex-3-en-1-yl]acetate, a pale yellowish oil, had the molecular formula $C_{29}H_{42}O_5$ deduced from HRESIMS (obsd. $[M + Na]^+ - H_2O$ at *m/z* 475.2842, theor. $[M + Na]^+ - H_2O$ = 475.2819 and $[2\,M + Na]^+ - H_2O$ at *m/z* 927.5725, theor. $[2\,M + Na]^+ - H_2O$ = 927.5751). The specific rotation ($[\alpha]_D^{23}$) was established as + 54.0 (*c* 0.2, MeCN). For ^{1}H and ^{13}C data, see Table 1.

2.2.2. Melissifoliane B (2)

Melissifoliane B (2, RT ≈ 45 min), (*E*)-methyl-2-{3-[(*E*)-3,7-dimethylocta-2,6-dien-1-yl]-2,5-dihydroxyphenyl}-4-hydroxy-5,9-dimethyldeca-5,8-dienoate, a pale yellowish oil, had the molecular formula $C_{29}H_{42}O_5$ as deduced from HRESIMS results (obsd. $[M + Na]^+ - H_2O$ at *m/z* 475.2852, theor. $[M + Na]^+ - H_2O$ = 475. 2819 and $[2\,M + Na]^+ - H_2O$ at *m/z* 925.5530, theor. $[2\,M + Na]^+ - H_2O$ =927.5751). For ^{1}H and ^{13}C data, see Table 1.

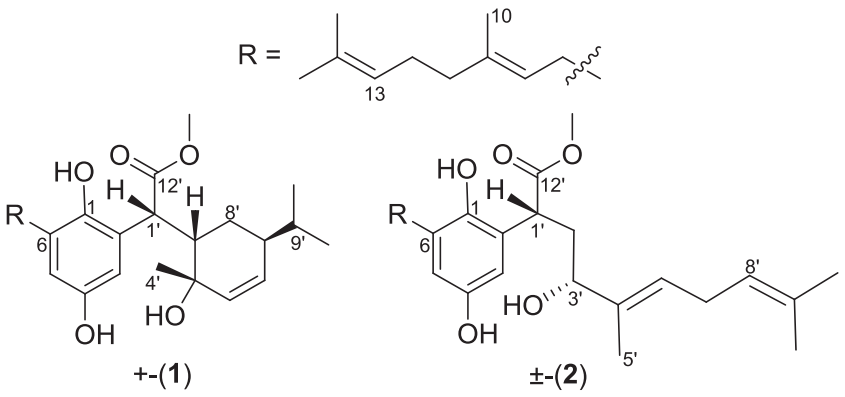

Fig. 1. Structure of melissifolianes A (1) and B (2).

Table 1
^{1}H and ^{13}C NMR data of melissifolianes A and B (1 and 2). The numberings shown in this table are not consistent with the systematic nomenclature for melissifolianes A and B (1 and 2) to expedite discussions.

	1		2	
	^{1}H (multi, *J* in Hz)	^{13}C	^{1}H (multi, *J* in Hz)	^{13}C (multi)
1		144.2		146.9
2		117.0		118.8
3	6.56 (1H, br d, 2.6)	113.3	6.47 (1H, br d, 2.9)	111.3
4		148.4		148.5
5	6.58 (1H, br d, 2.4)	115.8	6.57 (1H, br d, 2.7)	115.8
6		131.2		131.3
7	3.31, 3.18 (2H, dd, 14.9, 7.5)	28.3	3.27 (2H, d, 7.5)	28.1
8	5.28 (1H, t, 7.03)	122.2	5.30 (1H, t, 7.5)	121.9
9		136.1		136.4
10	1.69 (3H, s)	16.2	1.68 (3H, s)	16.1
11	2.04 (2H, m)	39.8	2.05 (2H, m)	39.8
12	2.10 (2H, m)	26.7	2.12 (2H, m)	26.7
13	5.12 (1H, t, 5.9)	124.4	5.13 (1H, t, 7.6)	124.3
14		131.3		131.4
15	1.70 (3H, s)	25.7	1.70 (3H, s)	25.7
16	1.62 (3H, s)	17.7	1.62 (3H, s)	17.7
1′	4.15 (1H, d, 6.2)	43.3	3.98 (1H, dd, 11.3, 6.4)	42.8
2′	2.28 (1H, ddd, 13.9, 6.1, 2.9)	35.4	2.26, 2.19 (2H, m)	30. 5
3′		72.3	4.27 (1H, dd, 10.70, 3.69)	79.4
4′	1.33 (3H, s)	24.6		134.0
5′	5.80 (1H, d, 9.9)	131.7	1.77 (3H, s)	12.2
6′	5.97 (1H, dd, 9.9, 4.6)	134.0	5.53 (1H, t, 7.1)	126.4
7′	1.93 (1H, m)	40.8	2.79 (2H, t, 6.9)	26.7
8′	1.63, 1.37 (2H, m)	23.2	5.13 (1H, t, 6.8)	122.3
9′	1.66 (1H, m)	31.7		132.1
10′	0.93 (3H, d, 6.7)	20.9	1.66 (3H, s)	17.8
11′	0.98 (3H, d, 6.5)	21.0	1.72 (3H, s)	25.7
12′		173.4		174.1
13′	3.83 (3H, s)	51.9	3.77 (3H, s)	52.2

2.3. QM computational calculation

2.3.1. ECD calculation

Initial conformational analysis was conducted using the Amber* force field in the MacroModel program included in the Schrödinger software package (Schrödinger LLC.). Four dihedral angles were set to the initial values shown in Table S2-1. The resulting structures were subsequently optimized using the PM6 semi-empirical method in the Gaussian 09 package (Gaussian Inc.). The PM6-optimized structures were further optimized using density-functional theory (DFT) gas-phase calculations and the resulting dihedral angles for the conformations are listed in Table S2-1. The geometry optimizations and frequency calculations of the Conformers 1–24 (See Supplementary data 2) were conducted by using the hybrid DFT method B3LYP with the 6-31G(d,p) basis set, specifying tight convergence. The major conformers (Conformers 1, 3, 5, 6, 13, 14, 15, 16, 17 and 19) from the optimization process were further minimized using B3LYP/6-311++G(2d,p) with tight convergence in order to demonstrate the effects of including a larger basis set. Separate optimizations were carried out starting from the PM6-optimized structures, using the Conductor-like Polarizable Continuum solvation Model (CPCM) with a dielectric constant representing MeCN, and the resulting dihedral angles for the conformations are listed in Table S2-5. The excited state calculations were performed using the time-dependent DFT (TDDFT) method using B3LYP with each of the two basis sets. The generated excitation energies and rotational strengths were weighted using Boltzmann averaging based on the calculated Gibbs free energy of each conformer and then fitted using a Gaussian function to generate the computed ECD spectra, utilizing SpecDis [10], for comparison to experiment.

2.3.2. Spin–spin coupling constant (SSCC) calculation

Geometries were optimized in Jaguar (Schrödinger LLC.) using DFT at the MPW1PW91/6-31G(d,p) level for all six staggered rotamers of each diastereomer associated with C-1′–C-2′ of melissifolianes A and B (1 and 2) (Fig. 5). The SSCC of each rotamer was calculated using the same theory and basis set in Gaussian09 [11]. The total absolute deviation (TAD) [12,13] between experimental and calculated values was used to suggest the most relevant conformers, and by extension of the empirical results, their configuration.

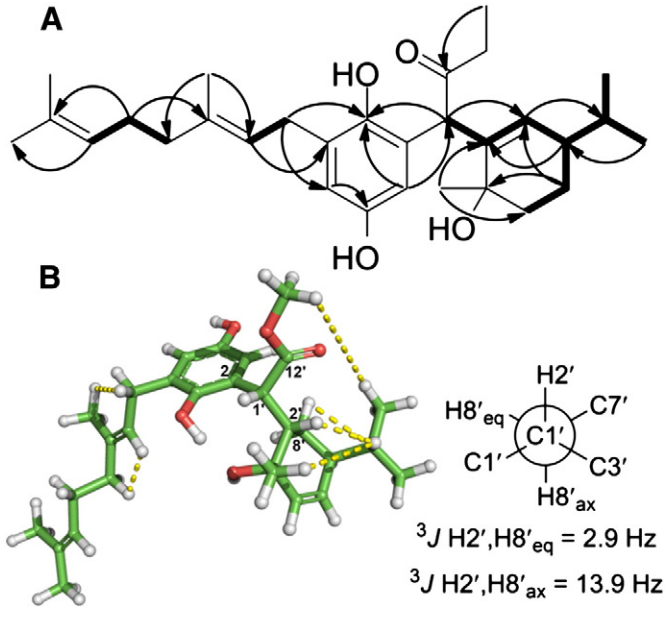

Fig. 2. (A) Key HMBC (arrows) and COSY (bold lines) and (B) Key NOEs (dotted lines) of melissifoliane A (1).

3. Results and discussion

The ^{1}H NMR spectrum of melissifoliane A (1) (Fig. S1-2, Table 1) showed signals for isopropyl protons (δ_H 0.98, 0.93), two *m*-coupled aromatic protons (δ_H 6.58, 6.56) and three tertiary and one secondary methyl protons (δ_H 1.70, 1.33, 1.63, 1.69). Downfield methyl protons were observed at δ_H 3.83, suggesting a methyl ester functional group supported by an HMBC correlation between the protons and ester carbonyl at δ_C 173.4. The ^{13}C NMR spectrum deduced from the HSQC spectrum (Fig. S1-5) revealed a benzene ring bearing two oxygenated carbons (δ_C 148.4, 144.2, 131.2, 117.0, 115.8, 113.3). HMBC and COSY spectra analyses revealed that the gross structure of melissifoliane A (1) was based on a 2-(hydroquinone) acetic acid ester moiety flanked by two monoterpene units (Fig. 2A). The connectivity between the cyclic monoterpene and 2-(hydroquinone) acetic acid ester was confirmed by the COSY correlation between H-1′ (δ_H 4.15) and H-2′ (δ_H 2.28) and the HMBC correlations between H-1′ and C-8′ (δ_C 23.2), and H-3 (δ_H 6.56) and C-1′ (δ_C 43.3) (Fig. 2A). The acyclic terpene unit was similarly connected to C-6 of the hydroquinone moiety via the COSY correlation of H-7 (δ_H 3.31, 3.18) and H-8 (δ_H 5.28), and the HMBC correlations H-8 and C-6 (δ_C 131.2), H-7 and C-5 (δ_C 115.8), and H-7 and C-1 (δ_C 144.2) (Fig. 2A). The relative configuration of melissifoliane A (1) was established by assignment of ^{1}H–^{1}H NOE and QM calculation approaches combined with computational modeling. The (*E*) C-8–C-9 olefin geometry was assigned based on a characteristic pair of carbon resonances for the C-10 methyl and the C-11 methylene at δ_C 16.2 and 39.8, respectively and NOE crosspeaks between H_2-7 (δ_H 3.31, 3.18) and H_3-10 (δ_H 1.69), and H-8 (δ_H 5.28) and H_2-11 (δ_H 2.04) (Fig. 2B). The relative configuration of the cyclic monoterpene unit was established based on the NOE correlations between H-2′ (δ_H 2.28) and H-9′ (δ_H 1.66), H-4′ (δ_H 1.33) and H-9′, and H-8′ (δ_H 1.63, 1.37) and

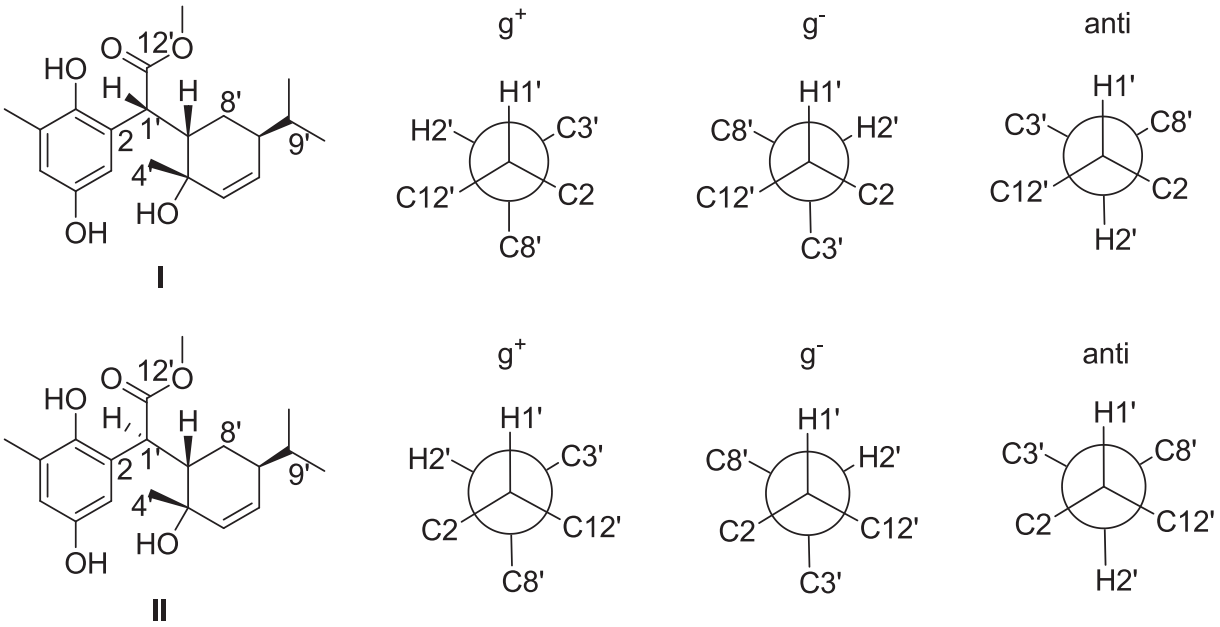

Fig. 3. Diastereomers I and II, the representative structures of melissifoliane A (1) with different C-1′ configurations along with the Newman projections demonstrating all possible staggered rotamers associated with C-1′–C-2′ bond.

H-9′. $^{3}J_{H\text{-}2',H\text{-}8'ax}$ (13.9 Hz) and $^{3}J_{H\text{-}2',H\text{-}8'eq}$ values (2.9 Hz) suggesting the cyclohexene ring was in the half-chair conformation. The orientation of the isopropyl group was validated by the NOE between H-11′ (δ_H 0.98) and the methyl ester group, H-13′ (δ_H 3.83). Thus, the relative configuration of the monoterpene unit was tentatively assigned 2′*S**, 3′*S**, and 7′*S**.

The observed $^{3}J_{H1',H2'}$ value (6.2 Hz) indicated a conformational assemblage in which anti- and gauche-conformers around the C-1′–C-2′ bond predominated, thus making the assignment of C-1′ configuration challenging. The NMR and QM combined approach utilized the comparison between experimental and calculated spin–spin coupling constants (SSCCs) to establish the relative configuration of C-1′. Geometries were optimized in Jaguar (Schrödinger LLC.) using DFT at the MPW1PW91/6-31G(d,p) level for all six staggered rotamers associated with the C-1′–C-2′ bond of each diastereomer having different C-1′ configurations (Fig. 5). The SSCCs of each rotamer were calculated using the same theory and basis set in Gaussian09 (Table 2, Fig. 3). The total absolute deviation (TAD) [12,13] between the experimental and calculated values (Table 2, Fig. 3) suggested that the calculated SSCCs of diastereomer I in Fig. 3 with 1′*R**, 2′*S**, 3′*S**, 7′*S** showed a better agreement with the experimental *J* values.

The absolute configuration of melissifoliane A (1) was assigned by comparison of the calculated and experimental ECD spectra [14–21]. The major conformers were generated by selecting sensible dihedral angles for the rotamers around the C-6–C-7, C-2–C1′, C-1′–C-2′ and C-1′–C-12′ bonds. The cyclohexene ring was also restricted to a half-chair conformation as described above. The Amber* force field was used to define the initial geometries followed by PM6 [22] semi-empirical optimizations. These conformers were subsequently used in hybrid DFT B3LYP/6-31G(d,p) calculations to obtain more accurate geometries in the gas phase and in MeCN employing the Conductor-like Polarizable Continuum Model [23,24]. The 24 lowest-energy conformers (Conformer 1–24, see Supplementary data 2) within an energy

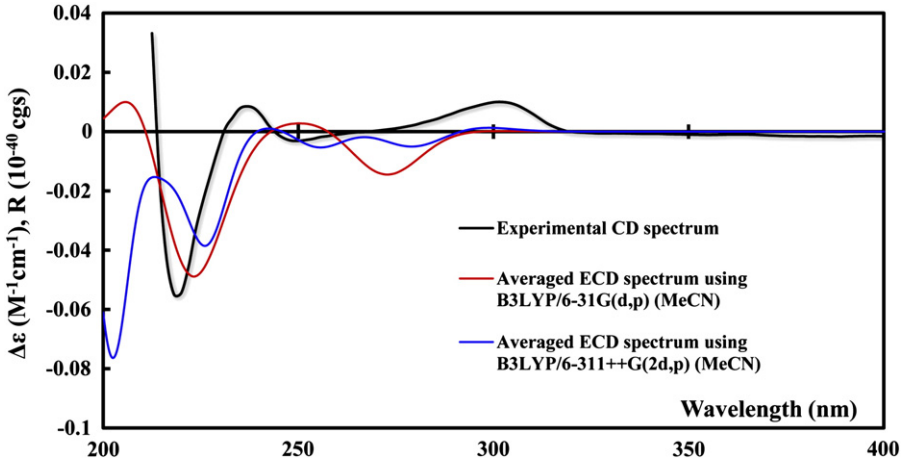

Fig. 4. Overlaid experimental and average calculated ECD spectra of melissifoliane A (1) utilizing the two different basis sets (see Supplementary data 2 for the details).

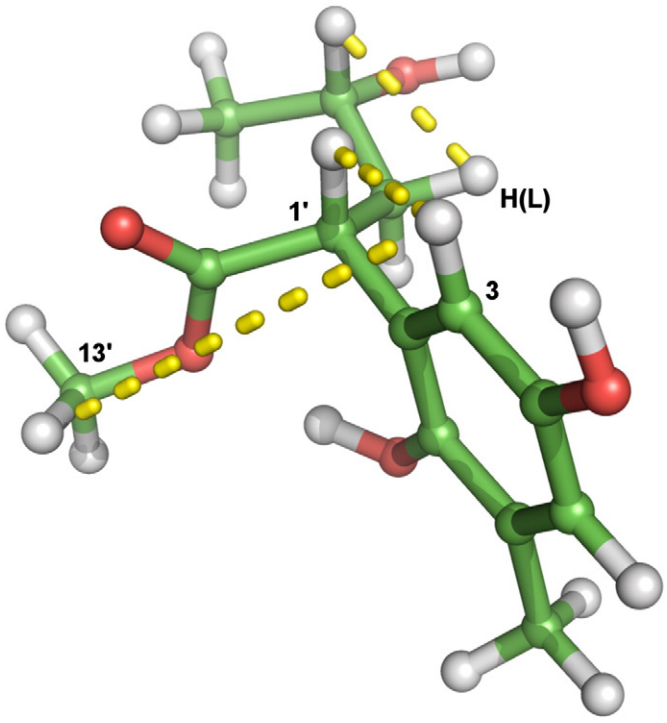

Fig. 5. DFT mPW1PW91/6-31G(d,p) geometry and energy-optimized gauche$^+$ conformer of melissifoliane B (2) diastereomer I in Fig. S1-22. Dotted lines indicate observed NOE. The use of a distance constraint obtained through the calibrated integration of NOE to H-3 of the hydroquinone ring orients the plane of the ring. The optimization for all the staggered rotamers of melissifoliane A (1) were achieved in the same manner.

window of 50 kJ/mol were compared to the minimum-energy conformer which exhibited different intramolecular hydrogen bond interactions, involving the C-1 and C-3′ hydroxy groups and the C-12′ ester oxygen atoms. Such hydrogen bonding interactions partially restricted rotation regarding the C-12′ – C-1′, C-1′ – C-2 and C-1′ – C-2′ bonds.

The full array of conformers was used for excited state TDDFT calculations in the gas phase and in MeCN. The excitation energies and rotational strengths of each conformer were Boltzmann weighted according to the calculated Gibbs free energies and subsequently fitted to Gaussian functions to simulate ECD curves. The major conformers found with B3LYP/6-31G(d,p) (see Section 2.3.1 and Supplementary data 2) were further optimized and then employed for ECD calculations utilizing B3LYP/6-311G++(2d,p) to validate the initial ECD calculations. The experimental ECD spectrum of melissifoliane A (1) shows Cotton effects characteristic of the $n \rightarrow \pi^*$ electronic transition of the ester functionality at *ca.* 300 nm, and the ^1L_b transition of the aromatic chromophore at *ca.* 260 nm and the ^1L_a transition of the aromatic chromophore in the 220–240 nm region (Fig. 4). Fig. 4 depicts overlays of the experimental spectrum of melissifoliane A (1), the average calculated spectrum of Conformers 1–24 and the average spectrum of the above-mentioned major conformers of melissifoliane A (1) using B3LYP/6-31G(d,p) and B3LYP/6-311++G(2d,p), respectively. The calculated data employing the different basis sets shown in Fig. 4, taken in conjunction with the experimental ECD curve, was sufficient to assign the absolute configuration as 1′*R*, 2′*S*, 3′*S*, 7′*S*.

The 1D NMR spectra of melissifoliane B (2) (Table 1, Fig. S1-11) resembled melissifoliane A (1), which suggested that it shared structural similarities with the exception of the nature of the methyl groups of the C-1′ acyclic substituent. The acyclic terpene and hydroxylated terpene moieties were connected to C-6 (δ_C 131.3) and C-1′ (δ_C 42.8) respectively, using similar COSY and HMBC correlations as described for melissifoliane A (1) (Fig. S1-13 and S1-15). The C-8 – C-9 olefin geometry was established as *E* based on the NOE crosspeaks between H_2-7 (δ_H 3.27) and H_3-10 (δ_H 1.68), and H-8 (δ_H 5.30) and H_2-11 (δ_H 2.05) (Fig. S1-16). The *E* geometry of the C-4′ – C-6′ olefinic bond was assigned by the chemical shift values of C3′ (δ_C 79.4) and C5′ (δ_C 12.2) and NOE crosspeaks between H_3-5′ (δ_H 1.77) and H_2-7′ (δ_H 2.79), and H-3′ (δ_H 4.27) and H-6′ (δ_H 5.53). Melissifoliane B was optically inactive which suggested a racemic mixture, and was subsequently confirmed by chiral chromatography (Fig. S1-23). Assignment of the relative configuration of melissifoliane B (2) using *J*-based analysis was limited by the lack of a relevant model for phenyl substituents and inadequate signal for the measurement of the $^3J_{CH}$ involving quaternary carbons of the hydroquinone moiety. Consequently, the relative configuration of melissifoliane B (2) was also assigned by the NMR and QM combined approach aided by the addition of relevant distance and conformational constraints determined through NOE's and conventional *J*-based analysis [25]. The gauche$^+$ conformer of diastereomer I in Fig. S1-21 exhibited the lowest TAD value (Table S1-1) and was assembled with the major conformer suggested by *J*-based analysis associated with C-2′ – C-3′ (Fig. 6), suggesting the relative configuration of melissifoliane B (2) as 1′*R** and 3′*R**.

Table 2
Calculated SSCCs (Hz) of the fragment of melissifoliane A (1) for the representative conformers associated with the C-1′ – C-2′ bond of the potential diastereomers together with the experimentally derived values which indicate the lowest TAD corresponding to diastereomer I.

	Calculated SSCC[a]						Exp.[b]
	I			II			
	g$^+$	g$^-$	anti	g$^+$	g$^-$	anti	
$^3J_{H1',H2'}$	3.9	5.0	6.9	4.1	4.1	9.3	6.2
$^3J_{H1',C8'}$	5.9	1.4	4.6	5.3	2.8	1.9	6.5
$^2J_{H1',C2'}$	−4.6	−1.5	−5.2	−1.8	−3.8	−1.9	−5.0
$^2J_{C1',H2'}$	−3.9	−4.0	−4.3	−3.3	−3.8	−4.4	−5.0
TAD	**4.4**	10.8	**3.5**	8.2	8.2	11.4	

TAD values calculated from ($\Sigma|J_{calc} - J_{exp}|$). I and II stand for the possible diastereomers having different C-1′ configurations of melissifoliane A (1). (See Fig. 3).Conformers displaying the lowest TAD values appear in bold.
[a] MPW1PW91/6-31G(d,p) calculated *J* values.
[b] Experimental *J* values observed from HETLOC and ^{1}H-NMR spectra.

4. Conclusion

Our study of the *L. melissifolia* metabolome exemplifies how new chemistry remains undiscovered among the numerous endangered plant species and demonstrates how analysis by ECD and NMR combined with various QM calculations is a valuable approach to support the stereochemical assignment of molecules with conformationally restricted conformations. Utilization of the secondary metabolites obtained from other endangered plant species may serve as added justification for conservation of such plants given they generate socioeconomic value.

Acknowledgement

We would like to recognize Mr. M. Brown (Bruker BioSpin) and Mr. W. Yoshida (The University of Hawaii) for NMR application expertise and the Mississippi Center for Supercomputing Research for supercomputer access. This investigation was conducted in a facility constructed with support from research facilities improvement program C06 RR-14503-01 from the NIH National Center for Research Resources. Research reported in this publication was also supported by the National Center For Complementary & Alternative Medicine of the National Institutes of Health under Award Number R01AT007318. The content is solely the responsibility of the authors and does not necessarily represent the official views of the National Institutes of Health.

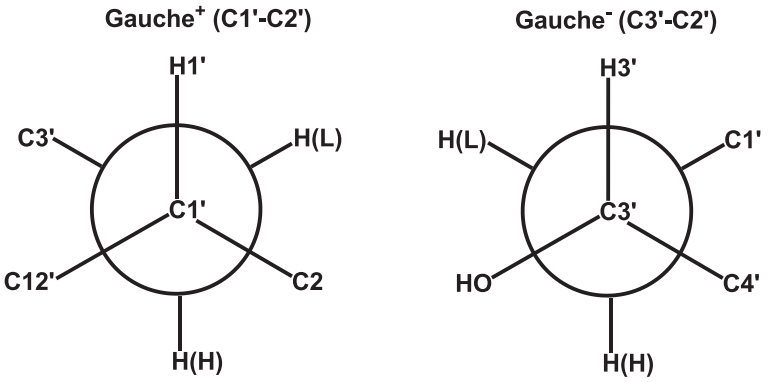

	Gauche+ (C-1'–C-2')	
	Calcd. SSCC[a]	Exp.[b]
$^3J_{H1', H(H)}$	11.3	11
$^3J_{H1', H(L)}$	3.2	5.2
$^3J_{H1', C3'}$	2.9	1.5
$^2J_{C1', H(H)}$	-3	-4
$^2J_{C1', H(L)}$	-3.1	-4
TAD	**5.6**	

	Gauche- (C-3'–C-2')
	Exp.[b]
$^3J_{H(H), H3'}$	10.7
$^3J_{H(L), H3'}$	3.7
$^3J_{H3', C1'}$	3
$^2J_{H(H), C3'}$	-6
$^2J_{H(L), C3'}$	-4

Fig. 6. The major conformers suggested by QM calculation (C-1′ – C-2′, left) (see Table S1-1 and Fig. S1-21) and *J*-based analysis (C-3′ – C-2′, right). $\delta_{H(H)}$ and $\delta_{H'(L)}$ indicate 2.26 and 2.19, respectively. [a]MPW1PW91/6-31G(d,p) calculated *J* values. [b]Experimental *J* values observed from HETLOC and 1-D ^{1}H-NMR spectrum. TAD: see Table 2. The geometry of melissifoliane B (2) was optimized as shown in Fig. 5. SSCCs of each C-1′ – C-2′ staggered rotamer were calculated in a manner identical to that completed for melissifoliane A (1).

Appendix A. Supplementary data

Supplementary data including additional NMR and HRMS spectra for melissifolianes A and B, HPLC chromatograms, and the details of the coupling constant calculations (Supplementary data 1) and the theoretical ECD calculations including coordinates (Supplementary data 2) can be found online at http://dx.doi.org/10.1016/j.bbagen.2013.04.029.

References

[1] F. Zhu, C. Qin, L. Tao, X. Liu, Z. Shi, X. Ma, J. Jia, Y. Tan, C. Cui, J. Lin, C. Tan, Y. Jiang, Y. Chen, Clustered patterns of species origins of nature-derived drugs and clues for future bioprospecting, Proc. Natl. Acad. Sci. U. S. A. 108 (2011) 12943–12948.
[2] N.C.A. Pitman, P.M. Jørgensen, Estimating the size of the world's threatened flora, Science 298 (2002) 989.
[3] USDA, http://plants.usda.gov/threat.html, (accessed 4/10/2011).
[4] Y. Meng, A.J. Krzysiak, M.J. Durako, J.I. Kunzelman, J.L.C. Wright, Flavones and flavone glycosides from *Halophila johnsonii*, Phytochemistry 69 (2008) 2603–2608.
[5] S.E. Binns, J. Hudson, S. Merali, J.T. Arnason, Antiviral activity of characterized extracts from *echinacea* spp. (Heliantheae: Asteraceae) against virus (HSV-I), Planta Med. 68 (2002) 780–783.
[6] F.G. Braga, M.L.M. Bouzada, R.L. Fabri, M. de O. Matos, F.O. Moreira, E. Scio, E.S. Coimbra, Antileishmanial and antifungal activity of plants used in traditional medicine in Brazil, J. Ethnopharmacol. 111 (2007) 396–402.
[7] M.A.B. Rajeh, Z. Zuraini, S. Sasidharan, L.Y. Latha, S. Amutha, Assessment of *Euphorbia hirta* L. leaf, flower, stem and root extracts for their antibacterial and antifungal activity and brine shrimp lethality, Molecules 15 (2010) 6008–6018.
[8] J. Oh, J.J. Bowling, J.F. Carroll, B. Demirci, K.H.C. Başer, T.D. Leininger, U.R. Bernier, M.T. Hamann, Natural product studies of U.S. endangered plants: volatile components of *Lindera melissifolia* (Lauraceae) repel mosquitoes and ticks, Phytochemistry 80 (2012) 28–36.
[9] T. Noshita, H. Kiyota, Y. Kidachi, K. Ryoyama, S. Funayama, K. Hanada, T. Murayama, New cytotoxic phenolic derivatives from matured fruits of *Magnolia denudata*, Biosci. Biotechnol. Biochem. 73 (2009) 726–728.
[10] T. Bruhn, Y. Hemberger, A. Schaumloffel, G. Bringmann, SpecDis, Version 1.51, University of Wuerzburg, Germany, 2011.
[11] G. Bifulco, C. Bassarello, R. Riccio, L. Gomez-Paloma, Quantum mechanical calculations of NMR *J* coupling values in the determination of relative configuration in organic compounds, Org. Lett. 6 (2004) 1025–1028.
[12] A. Plaza, G. Bifulco, M. Masullo, J.R. Lloyd, J.L. Keffer, P.L. Colin, J.N.A. Hooper, L.J. Bell, C.A. Bewley, Mutremdamide A and koshikamides C– H, peptide inhibitors of HIV-1 entry from different *Theonella* species, J. Org. Chem. 75 (2010) 4344–4355.
[13] A. Plaza, R. Garcia, G. Bifulco, J.P. Martinez, S. Hüttel, F. Sasse, A. Meyerhans, M. Stadler, R. Müller, Aetheramides A and B, potent HIV-inhibitory depsipeptides from a myxobacterium of the new genus "*Aetherobacter*", Org. Lett. 14 (2012) 2854–2857.
[14] S. Abbate, A. Ciogli, S. Fioravanti, F. Gasparrini, G. Longhi, L. Pellacani, E. Rizzato, D. Spinelli, P.A. Tardella, Solving the puzzling absolute configuration determination of a flexible molecule by vibrational and electronic circular dichroism spectroscopies and DFT calculations: the case study of a chiral 2,2′-dinitro-2,2′-biaziridine, Eur. J. Org. Chem. 2010 (2010) 6193–6199.
[15] G. Bringmann, T. Bruhn, K. Maksimenka, Y. Hemberger, The assignment of absolute stereostructures through quantum chemical circular dichroism calculations, Eur. J. Org. Chem. 2009 (2009) 2717–2727.
[16] M. Woźnica, A. Butkiewicz, A. Grzywacz, P. Kowalska, M. Masnyk, K. Michalak, R. Luboradzki, F. Furche, H. Kruse, S. Grimme, J. Frelek, Ring-expanded bicyclic β-lactams: a structure–chiroptical properties relationship investigation by experiment and calculations, J. Org. Chem. 76 (2011) 3306–3319.
[17] G. Bencivenni, L.-Y. Wu, A. Mazzanti, B. Giannichi, F. Pesciaioli, M.-P. Song, G. Bartoli, P. Melchiorre, Targeting structural and stereochemical complexity by organocascade catalysis: construction of spirocyclic oxindoles having multiple stereocenters, Angew. Chem. 121 (2009) 7336–7339.
[18] P.L. Polavarapu, G. Scalmani, E.K. Hawkins, C. Rizzo, N. Jeirath, I. Ibnusaud, D. Habel, D.S. Nair, S. Haleema, Importance of solvation in understanding the chiroptical spectra of natural products in solution phase: garcinia acid dimethyl ester, J. Nat. Prod. 74 (2010) 321–328.
[19] M. Kwit, M.D. Rozwadowska, J. Gawroński, A. Grajewska, Density functional theory calculations of the optical rotation and electronic circular dichroism: the absolute configuration of the highly flexible trans-isocytoxazone revised, J. Org. Chem. 74 (2009) 8051–8063.
[20] J.-M. Gao, J.-C. Qin, G. Pescitelli, S. Di Pietro, Y.-T. Ma, A.-L. Zhang, Structure and absolute configuration of toxic polyketide pigments from the fruiting bodies of the fungus *Cortinarius rufo-olivaceus*, Org. Biomol. Chem. 8 (2010) 3543–3551.
[21] J. Dai, K. Krohn, U. Flörke, G. Pescitelli, G. Kerti, T. Papp, K.E. Kövér, A.C. Bényei, S. Draeger, B. Schulz, T. Kurtán, Curvularin-type metabolites from the fungus *Curvularia* sp. isolated from a marine alga, Eur. J. Org. Chem. 2010 (2010) 6928–6937.
[22] J. Stewart, Optimization of parameters for semiempirical methods V: modification of NDDO approximations and application to 70 elements, J. Mol. Model. 13 (2007) 1173–1213.
[23] M. Cossi, N. Rega, G. Scalmani, V. Barone, Energies, structures, and electronic properties of molecules in solution with the C-PCM solvation model, J. Comput. Chem. 24 (2003) 669–681.
[24] J. Wang, W.-Z. Zhai, Y. Zou, J.-J. Zhu, J. Xiong, Y. Zhao, G.-X. Yang, H. Fan, M.T. Hamann, G. Xia, J.-F. Hu, Eucalyptals D and E, new cytotoxic phloroglucinols from the fruits of *Eucalyptus globulus* and assignment of absolute configuration, Tetrahedron Lett. 53 (2012) 2654–2658.
[25] N. Matsumori, D. Kaneno, M. Murata, H. Nakamura, K. Tachibana, Stereochemical determination of acyclic structures based on carbon–proton spin-coupling constants. A method of configuration analysis for natural products, J. Org. Chem. 64 (1999) 866–876.